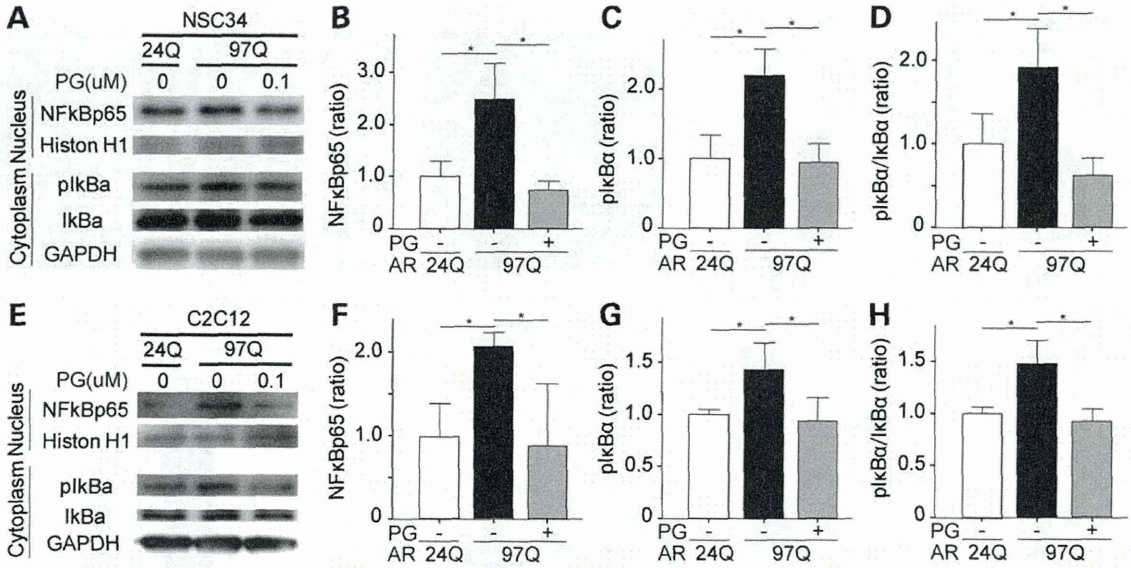

Figure 5. Effect of PG on NFκB signals in cellular model of SBMA. (**A**–**H**) Immunoblots of nuclear NFκBp65, cytoplasmic pIκBα and IκBα in NSC34 (A–D) and C2C12 cells (E–H) transfected with tAR-24Q or tAR-97Q and treated with or without PG. Quantitative analyses were performed using the densitometry of NFκBp65 (B, F), pIκBα (C, G) and the ratio of pIκBα to IκBα (D, H) ($n = 3$ per group). Error bars indicate s.e.m. * $P < 0.05$ by ANOVA with Dunnett's test (B–D, F–H).

to healthy tissue. Therefore, we investigated the state of microglia and the effects of PG on these cells in AR-97Q mice. Immunohistochemical analyses showed that cells in the anterior horn of the spinal cords of untreated AR-97Q mice had more microglia that were positive for CD86, an M1 glial cell surface marker, than the corresponding cells in wild-type mice; however, this phenomenon was mitigated by PG treatment (Fig. 7A, B). In contrast, PG increased immunoreactivity against Arg1, an M2 glial marker, in the microglia of the anterior horn of the spinal cords of AR-97Q mice; untreated AR-97Q mice had decreased immunoreactivities to Arg1 (Fig. 7C, D). Immunohistochemistry using anti-Iba1, a general microglial marker, demonstrated little difference in the levels of this marker among wild-type, untreated AR-97Q and PG-treated AR-97Q mice (Fig. 7E, F). Similar findings were observed in immunoblot analyses of the anterior part of the spinal cords of 13-week-old mice (Fig. 7G–J). The M1/M2 ratio was therefore markedly higher in the microglia of the anterior horn of the spinal cords of untreated AR-97Q mice than in those of wild-type mice. However, the M1/M2 ratio was restored to normal levels by PG treatment, suggesting that the release of proinflammatory molecules is associated with the pathogenesis of SBMA. In addition, PG treatment induced the phenotypic conversion of microglia from a proinflammatory M1 state to an anti-inflammatory M2 state, which is associated with neuroprotection. The results of immunohistochemical analyses revealed that there were more CD86-positive macrophages in the skeletal muscles of untreated AR-97Q mice than those of wild-type mice, and this phenomenon was suppressed by PG treatment (Supplementary Material, Fig. S14A). In contrast, PG increased the number of Arg1-positive macrophage in the skeletal muscles of AR-97Q mice; untreated AR-97Q mice had less immunoreactivities to Arg1 compared with wild-type mice (Supplementary Material, Fig. S14B).

The expression of genes related to inflammation is significantly altered in the spinal cord and muscle of PG-treated AR-97Q mice

To understand the global molecular changes induced by the administration of PG, we prepared total mRNA samples from the spinal cords and skeletal muscles of 13-week-old untreated AR-97Q and PG-treated AR-97Q mice and performed gene expression analyses. The microarray analyses found that the expression levels of 83 genes and 422 genes were significantly increased (>2-fold and >3-fold, respectively) in the spinal cords and skeletal muscles, respectively, of PG-treated mice ($P < 0.05$) (Supplementary Material, Fig. S15, S16). We then performed functional analysis using gene ontology (GO) of these genes, classifying them into several functional categories: immune response, extracellular matrix, cell adhesion, metabolism and others (Fig. 8A, B). As for the down-regulated genes, there were no GO terms, the frequency of which was found to be significantly decreased (less than one-half in the spinal cords and less than one-third in the skeletal muscles). Genes related to the immune response and extracellular matrix were predominantly altered by PG treatment, suggesting that the PPARγ agonist modulates the inflammatory response (especially along the NFκB pathway). The results also demonstrated that genes from similar functional categories are found in the spinal cord and skeletal muscle, indicating that PG attenuates the toxicity of polyglutamine-expanded AR in both neural and muscular tissues via a similar mechanism (Supplementary Material, Fig. S17A, B).

DISCUSSION

Recent studies have shown that mitochondrial dysfunction and oxidative stress-mediated neuronal toxicity are implicated in

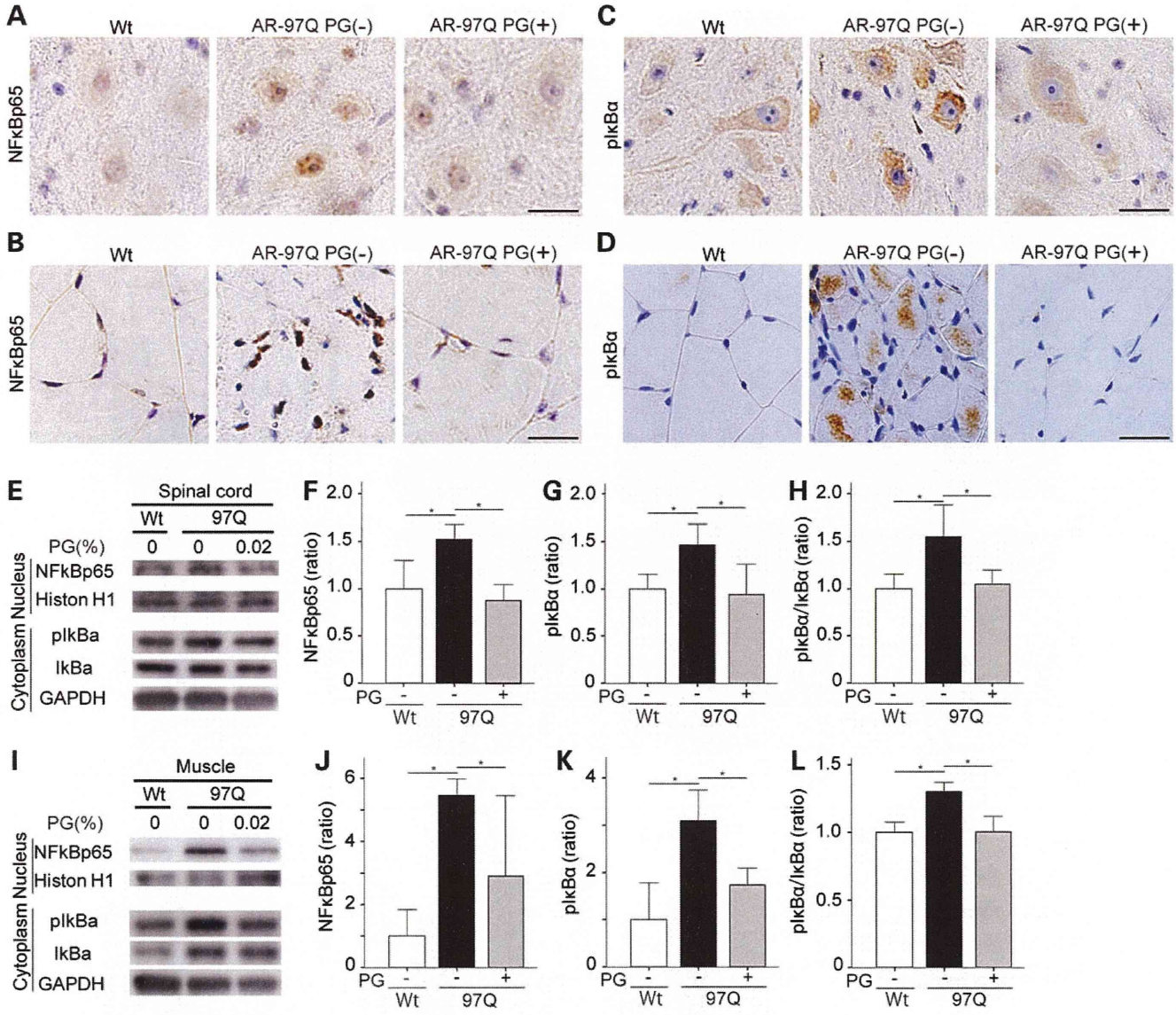

Figure 6. Effect of PG on NFκB signals of SBMA mice. (**A–D**) Immunohistochemistry for NFκBp65 (A, B) and pIκBα (C, D) in 13-week-old mice. (**E–L**) Immunoblots for nuclear NFκBp65, cytoplasmic pIκBα and IκBα in the spinal cords (E–H) and skeletal muscles (I–L) of 13-week-old mice. Quantitative analyses were performed using the densitometry of NFκBp65 (F, J), pIκBα (G, K) and the ratio of pIκBα to IκBα (H, L) ($n = 3$ per group). Error bars indicate s.e.m. * $P < 0.05$ by ANOVA with Dunnett's test (F–H, J–L). Error bars indicate s.e.m. * $P < 0.05$ by ANOVA with Dunnett's test (F–H, J–L). Scale bars: 25 μm (A–D).

various neurodegenerative diseases, including Huntington's disease, amyotrophic lateral sclerosis (ALS) and Friedreich's ataxia (30–35). In the present study, we demonstrated that the mRNA and protein levels of PPARγ, a regulator of mitochondrial function, were decreased in mouse and cellular models of SBMA. The results of reporter assay showed that the pathogenic AR suppressed the activity of *PPARγ* promoter. The mRNA levels of PGC1α, the co-activator of PPARγ, were also down-regulated in the spinal cord of our mouse model of SBMA, as reported in another mouse model of this disease (17). Decreased mRNA expression of PGC1α and PGC1α-regulated factors is also reported in the ALS mouse model and in human sporadic ALS, suggesting that mitochondrial dysfunction is a common pathological feature of motor neuron diseases (36,37). We also demonstrated that the overexpression of PPARγ and the administration of PG, a PPARγ agonist, improved the viability of cellular models of SBMA. Moreover, the oral administration of PG to SBMA mice improved neurological symptoms and histopathological findings. Pioglitazone mitigated oxidative stress, mitochondrial dysfunction and the activation of the NFκB pathway in mouse and cellular models of SBMA, providing a mechanistic basis for this treatment. In addition, PG modulated microglial populations in the spinal cord of the SBMA mice. These findings suggest that the PPARγ pathway can inhibit oxidative stress, the NFκB pathway and inflammation in SBMA.

PPARγ agonists have been proven effective in mouse and cellular models of neurodegenerative disorders, trauma and stroke (21,24,27,38–45). For example, PG has been shown to

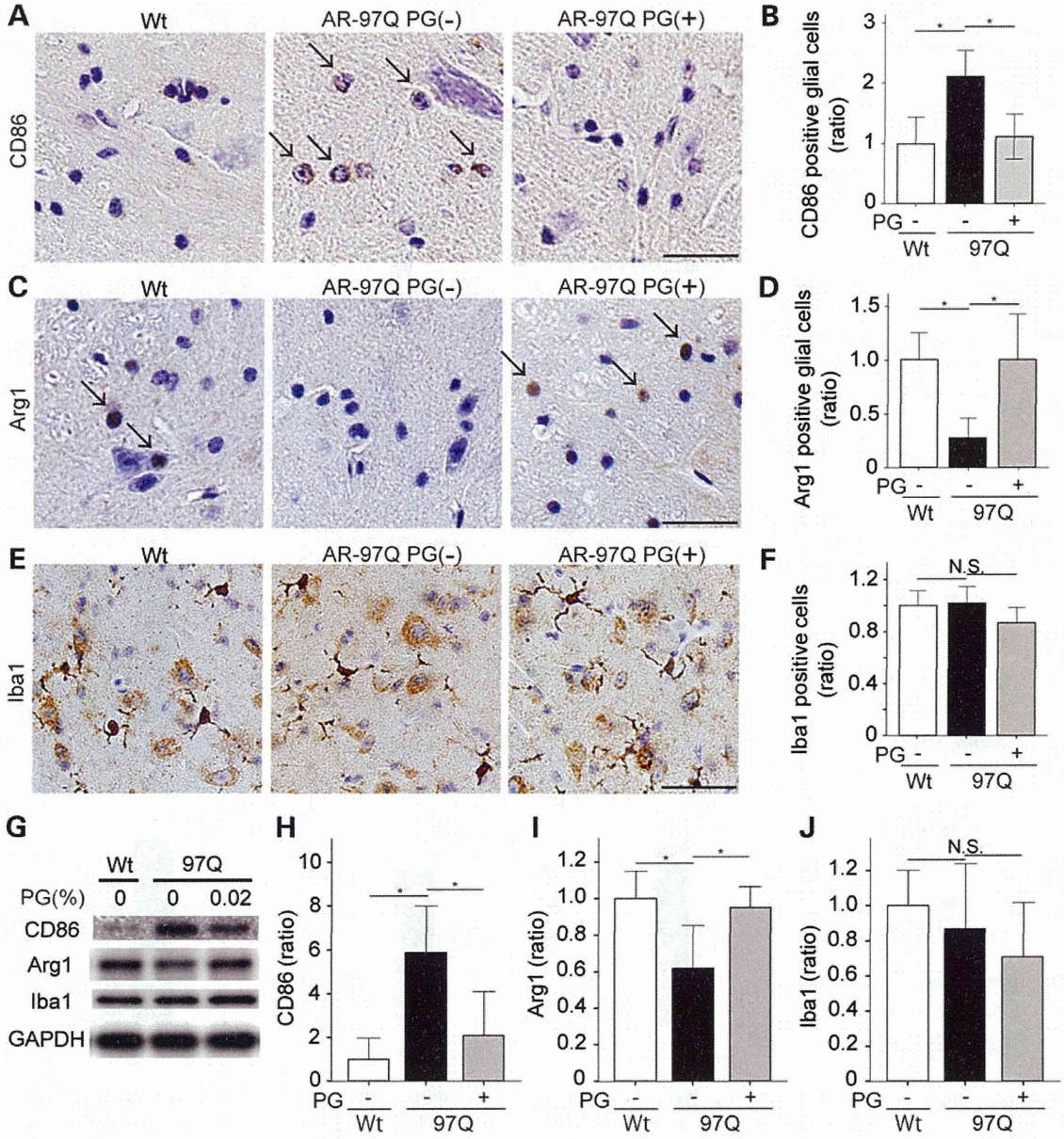

Figure 7. Effect of PG on the microglia of SBMA mice. (**A**–**F**) Immunohistochemistry with quantitative analyses of CD86 (A, B), Arg1 (C, D) and Iba1 (E, F) in 13-week-old mice. The arrows indicate the CD86- (A) and Arg1- (C) positive cells. Quantitative analyses of the ratio of CD86- (B), Arg1- (D) and Iba1- (F) positive cells in the anterior horn were performed with $n = 3$ per group. (**G**) Immunoblots for CD86, Arg1 and Iba1 in the anterior part of the spinal cord from 13-week-old mice. (**H**–**J**) Quantitative analysis using densitometry of CD86 (H), Arg1 (I) and Iba1 (J) ($n = 3$ per group). Error bars indicate s.e.m. * $P < 0.05$ by ANOVA with Dunnett's test (B, D, F, H–J). N.S., not significant. Scale bars: 25 μm (A, C, E).

be neuroprotective in the G93A SOD1 transgenic mouse model of ALS (38), improving motor performance and increasing survival by reducing microglial activation and gliosis. Despite the promising preclinical trials using SOD1 mouse model, PG had no beneficial effects on the survival of ALS patients as add-on therapy to riluzole, indicating the difficulty of the translation from mouse models to human (46).

Pioglitazone has also been shown to reduce iNOS, NFκB and 3-nitrotyrosine immunoreactivity, and several of these findings were replicated in the present study. Pioglitazone treatment also improved motor function and mitigated oxidative stress and mitochondrial enzyme activity in a rat model of Huntington's disease induced by quinolinic acid (40). However, the administration of rosiglitazone to R6/2 transgenic Huntington's disease mice did not alter the course of survival or weight loss of the animals, possibly because insufficient levels of rosiglitazone were administered to sustain effective therapeutic levels or prevent rapid neurodegeneration (47).

Interestingly, in the present study, similar molecular changes related to oxidative stress and NFκB activation were observed in the motor neurons and skeletal muscles of SBMA mice. Microarray analyses showed that PG mitigated

A

GO term (spinal cord)	p value
collagen biosynthetic process	1.94E-03
collagen metabolic process	2.69E-03
proteinaceous extracellular matrix	2.69E-03
multicellular organismal macromolecule metabolic process	2.69E-03
multicellular organismal metabolic process	3.46E-03
extracellular matrix	4.12E-03
extracellular matrix structural constituent	4.37E-02

immune response
cell adhesion
extracellular matrix
metabolism

B

GO term (skeletal muscle)	p value
extracellular matrix	2.12E-28
extracellular region	1.20E-26
extracellular region part	1.66E-25
proteinaceous extracellular matrix	1.73E-25
extracellular space	2.29E-17
collagen	6.65E-16
extracellular matrix part	3.69E-14
fibrillar collagen	3.87E-08
extracellular matrix organization	2.44E-07
extracellular matrix structural constituent	2.44E-07
immune system process	2.44E-07
extracellular structure organization	2.53E-07
cell adhesion	9.29E-07
biological adhesion	1.18E-06
collagen fibril organization	1.93E-06
heparin binding	2.61E-06
glycosaminoglycan binding	3.26E-06
immune response	6.81E-06
protein heterotrimerization	1.80E-05
MHC class II protein complex	1.80E-05
carbohydrate derivative binding	1.83E-05
positive regulation of developmental process	5.89E-05
regulation of multicellular organismal process	5.89E-05
positive regulation of biological process	6.08E-05
antigen processing and presentation of exogenous peptide antigen	1.29E-04
antigen processing and presentation of exogenous peptide antigen via MHC class II	1.85E-04
sulfur compound binding	1.97E-04
plasma membrane part	2.24E-04
locomotion	3.93E-04
antigen processing and presentation of peptide antigen via MHC class II	4.06E-04
protein trimerization	4.06E-04
positive regulation of cellular process	4.49E-04
positive regulation of T cell activation	4.49E-04
antigen processing and presentation of exogenous	4.93E-04
antigen response to cytokine stimulus	6.29E-04
regulation of developmental process	7.18E-04
positive regulation of cell differentiation	7.18E-04
response to external stimulus	7.18E-04
antigen processing and presentation of peptide or polysaccharide antigen via MHC class II	7.18E-04
response to wounding	7.18E-04
cell activation	8.73E-04
regulation of defense response	9.11E-04
platelet-derived growth factor binding	9.29E-04
regulation of anatomical structure morphogenesis	9.32E-04
chemotaxis	9.77E-04

Figure 8. Gene ontology (GO) analysis. (**A**) The list of GO terms of the genes with expression levels that were significantly higher (>2-fold) in the spinal cords of PG-treated AR-97Q mice than in those of untreated AR-97Q mice at 13 weeks ($n = 3$ per group, $P < 0.05$). (**B**) The list of GO terms of the genes with significantly higher (>3-fold) expression levels in the skeletal muscles of PG-treated AR-97Q mice than in those of untreated AR-97Q mice at 13 weeks ($n = 3$ per group, $P < 0.05$).

these cellular events in both neuronal and muscular tissues. These effects were also observed in cellular experiments using neuronal and muscular cell lines. The results of the present study suggest that PG has direct effects on both neuronal and muscular degeneration in SBMA and that skeletal muscle is an important target for therapies that alleviate neuromuscular symptoms of SBMA.

Although we tested the ability of PG to modify mitochondrial function, our results also indicate that oxidative stress, the activation of the NFκB pathway and neuroinflammation play important roles in the pathogenesis of SBMA. Mitochondrial dysfunction, NFκB activation and the M1 microglial phenotype are known to be connected in several ways. For example, mitochondrial toxins caused by primary damage to the mitochondrial respiratory chain induce microglial activation and neuroinflammatory processes. Proinflammatory cytokines (such as tumor necrosis factor-α) released by M1 microglia alter the morphology and function of mitochondria (48,49). Furthermore, NFκB was recently identified as a physiological regulator of mitochondrial respiration, and NFκB-induced oxidative stress is thought to contribute to mitochondrial dysfunction in diabetic mice (50,51). NFκB activation in microglia also regulates inflammatory processes that exacerbate diseases such as ischemia and Alzheimer's disease (52). These findings implicate mitochondrial dysfunction, NFκB and microglial alteration in the pathogenesis of neurodegenerative diseases.

The results of the present study provide important insights into the NFκB-mediated pathogenesis of SBMA. The NFκB pathway was activated in the mouse and cellular models and in patients with SBMA. The overexpression of NFκBp50 or p65, key molecules of the signaling pathway, induced cellular damage in neuronal and muscular cells; however, PG treatment suppressed the activity of the NFκB pathway in the mouse and cellular models of SBMA. These findings suggest that NFκB signaling plays an important role in the pathogenesis of SBMA. NFκB activation has been implicated in the pathogenesis of various neurodegenerative disorders (35,53,54), and this pathway appears to be a commonly considered target of therapy for devastating neurological diseases.

Neuroinflammation is a common pathological feature of many neurodegenerative diseases and appears to play an important role in the non-cell autonomous pathogenesis (55,56) of several animal models of neurodegenerative disease. In animal models of ALS, lowering mutant superoxide dismutase 1 (SOD1) expression levels in microglia using the Cre–Lox recombination system significantly extended the survival of transgenic mice carrying a mutant human $SOD1^{G37R}$ gene (57–59). Moreover, microglia in the ALS mouse model appear to switch from an M2 state to an M1 state as the disease progresses (58,59). The present results suggest that PG exerts a neuroprotective effect on SBMA mice via the modulation of inflammation.

In conclusion, we demonstrated that PPARγ is down-regulated in SBMA and that the activation of this nuclear receptor by PG mitigates oxidative stress, NFκB activation and neuroinflammation and improves the symptoms and pathological findings of SBMA mice. Our results corroborate the decrease in PPARγ expression and the increases in oxidative stress and NFκB activity observed in autopsy samples from SBMA patients. Given that PG is already used as an oral-hyperglycemic drug and crosses the blood–brain barrier, this drug appears to be a safe and effective therapy for SBMA and other neurodegenerative diseases.

MATERIALS AND METHODS

Cell culture and transfection

Mouse NSC34 motor neuron-like cells (kindly provided by N.R. Cashman, University of British Columbia, Vancouver, Canada) and mouse C2C12 myoblast cells (DS Pharma Biomedical, Osaka, Japan) were cultured in a humidified atmosphere of 95% air/5% CO2 in a 37°C incubator in Dulbecco's Modified Eagle's Medium (DMEM) supplemented with 10% fetal bovine serum (FBS). DMEM/F12 with 10% FBS was used to culture SH-SY5Y human neuroblastoma cells (ATCC No. CRL-2266) and those stably expressing the human full-length AR-97Q. The plasmids were transfected using OPTI-MEM (Gibco, Germany) and Lipofectamine 2000 (Invitrogen, Carlsbad, CA, USA) according to the manufacturer's instructions. NSC34 cells were differentiated in DMEM for 96 h. Fetal horse serum (2%) was added to the medium for 48 h to differentiate the C2C12 cells. SH-SY5Y cells were differentiated in DMEM/F12 supplemented with 2% FBS and 20 μM retinoic acid. SH-SY5Y cells stably expressing AR-97Q were differentiated in DMEM/F12 supplemented with 20 μM retinoic acid and 1 nM 5α-dihydrotestosterone as described earlier (6).

Plasmid constructs and siRNA

The pEVRF-p65 vector encoding the murine RelA protein and the pCMV4-p50 vector encoding the NFκBp50 subunit were kindly provided by Drs. Genevieve Soucy and Jean-Pierre Julien (Department of Psychiatry and Neuroscience, Laval University, Research Centre of CHUL, Canada). The pcDNA3.1-PPARγ expression vector was cloned as previously described (60). The pCR3.1–AR–24Q and pCR3.1–AR–97Q plasmids were cloned as previously described (61). This truncated protein consisted of an N-terminal fragment of human *AR* containing 24 or 97 CAG repeats (1–645 bp and 1–864 bp, respectively) subcloned into pcDNA3.1 (6,62,63). To knock-down PPARγ, the following oligonucleotide siRNA duplexes were synthesized by Invitrogen and used to transfect the NSC34 and C2C12 cells: sense sequence, CAGAGCAAAGAGGUGGCCAUCCGAA; antisense sequence, UUCGGAUGGCCACCUCUUUGCUCUG. We used Stealth RNAi negative control duplex (Invitrogen) as the control siRNA. The NSC34 and C2C12 cells were transfected with the siRNA oligonucleotide duplex using Lipofectamine 2000 (Invitrogen) according to the manufacturer's instructions.

Cell viability, toxicity and apoptosis assays

The cell viability assays were performed using WST-8 (Roche Diagnostics, Mannheim, Germany). The cells were cultured in 24-well plates. Twenty-four hours after each treatment with the indicated concentrations of PG, the cells were incubated with the WST-8 substrate for 3–4 h and spectrophotometrically assayed at 450 nm using a plate reader (Powerscan HT, Dainippon Pharmaceutical, Osaka, Japan). The toxicity assays were performed using the Cytotoxicity Detection Kit PLUS (Roche Diagnostics, Indianapolis, IN). Twenty-four hours after the treatment, 100 μl of the medium was extracted from the plate and used for the assay. The medium was incubated with the substrate for 15 min and spectrophotometrically assayed at 490 nm using a plate reader. The number of dead cells was determined using a Countess cell counter (Invitrogen) after staining with trypan blue. For detecting apoptotic cells, we used Multi-Parameter Apoptosis Assay Kit (Cayman Chemical, MI, USA). The cells were cultured in 96-well black plates. After the treatment, plate reader fluorescence detection was performed according to the manufacturer's instructions.

Mitochondrial activity assay

The assessment of mitochondrial membrane potential was determined using MitoTracker™ green FM (Invitrogen) dyes. The dyes passively diffuse across the plasma membrane and accumulate in active mitochondria, whose accumulation is dependent upon membrane potential. The cells were incubated with 100 nM of the dyes for 30 min at 37°C in serum-free DMEM and washed with pre-warmed serum-free DMEM. The cells were then observed using a fluorescence microplate reader (Powerscan HT) at excitation and emission wavelengths of 490 and 516 nm, respectively.

Animals

AR-97Q (Line #7–8) male mice were bred and maintained as previously described (5,64). They have backcrossed at least 15 generations to C57BL/6 before used in the present study. The mice were genotyped by PCR using DNA from their tail (5). In the experiments, PG was administered at concentrations of 0.01 or 0.02% in the feed from 6 or 8 weeks of age until the end of the analysis, unless otherwise mentioned. Only males were used in this study. The litters were randomly allocated to PG-containing or normal chow. For pathological and biochemical analyses, the feed was administered to the mice beginning at 6 weeks of age.

Behavioral analysis

All of the tests were performed on a weekly basis, and the data were analyzed prospectively. The rotarod performance was assessed weekly using an Economex Rotarod (Ugo Basile, Comerio, Italy) as previously described (64). The grip strength was measured with a Grip Strength Meter (MK-380M, Muromachi Kikai, Tokyo, Japan) as described elsewhere (65).

Immunoblotting

Mice anesthetized with ketamine–xylazine were perfused with 4% paraformaldehyde fixative in phosphate buffer (pH 7.4). The tissues (whole brain, spinal cord, brainstem and skeletal muscle) were dissected and snap-frozen with powdered CO_2 in acetone. The tissues were homogenized in buffer containing 50 mM Tris–HCl (pH 8.0), 150 mM NaCl, 1% Nonidet P-40, 0.5% deoxycholate, 0.1% SDS and 1 mM 2-mercaptoethanol with Halt Protease and Phosphatase Inhibitor Cocktail (Thermo Scientific, Waltham, MA, USA) and centrifuged at 2500 × *g* for 15 min. The cultured cells were also lysed in the same reagent after intervention. NE-PER Nuclear Cytoplasmic Reagents (Thermo Scientific) were used for the analysis of the NFκB pathway. Equal amounts of protein were separated by 5–20% SDS–PAGE gels and transferred to Hybond-P membranes (GE Healthcare, Piscataway, NJ, USA). Primary antibody binding

was probed with horseradish peroxidase-conjugated secondary antibodies at a dilution of 1 : 5000, and the bands were detected using an immunoreaction enhancing solution (Can Get Signal; Toyobo, Osaka, Japan) and enhanced chemiluminescence (ECL Prime; GE Healthcare). An LAS-3000 imaging system (Fujifilm, Tokyo, Japan) was used to produce digital images. The signal intensities of these independent blots were quantified using IMAGE GAUGE software version 4.22 (Fuji) and expressed in arbitrary units. The membranes were reprobed with an anti-GAPDH (MAB374, 1 : 5000; Santa Cruz) antibody or Histone H1 (#05-457, 1 : 1000; Millipore, Billerica, MA, USA) for normalization.

Histology and immunohistochemistry

The mouse tissues were dissected, post-fixed in 10% phosphate-buffered formalin and processed for paraffin embedding. The sections to be stained with the anti-polyglutamine antibody (1C2) were treated with formic acid for 5 min at room temperature. The sections to be incubated with the anti-ChAT, GFAP, nitrotyrosine, pIκBα and Iba-1 antibodies were boiled in 10 mM citrate buffer for 15 min. The specificity of the monoclonal antibody against 8-OHdG (N45.1) has been characterized in a previous study (66). The sections to be incubated with the anti-8OHdG antibody were boiled in 0.1 M glycine buffer (pH 2.2) for 15 min. The sections to be incubated with an anti-NFκBp65 antibody were autoclaved using the 2100-Retriever (Funakoshi Corporation, Tokyo, Japan). Primary antibody binding was probed with a secondary antibody labeled with a polymer as part of the Envision+ system containing horseradish peroxidase (Dako Cytomation, Gostrup, Denmark). The immunohistochemical sections were photographed with an optical microscope (Axio Imager M1, Carl Zeiss AG, Göttingen, Germany). The immunoreactivity and cell sizes were analyzed with WinROOF (Mitani, Tokyo, Japan). The means ± s.e.m. were expressed in arbitrary units. For hematoxylin and eosin (H&E) staining, 6-μm-thick cryostat sections of the gastrocnemius muscles were air-dried and stained.

Quantitative analysis of immunohistochemistry

To assess 1C2-, CD86-, Arg1- and Iba1-positive cells, at least 50 consecutive 6-μm-thick axial sections of the thoracic spinal cord and skeletal muscle were prepared, and every fifth section was immunostained with each antibody. The numbers of 1C2-positive cells were counted in all of the neurons of the anterior horn of the 10 axial sections from the thoracic spinal cord of each group of mice ($n = 3$) under a light microscope (Bx51; Olympus, Tokyo, Japan). For the purposes of counting, we defined a motor neuron by its presence within the anterior horn and the obvious nucleolus in a given 6-μm-thick section. The numbers of 1C2-positive cells in skeletal muscles were calculated for >500 fibers in randomly selected areas of the 10 axial sections. To quantify the expression levels of nitrotyrosine, 8OHdG, NFκBp65 and pIκBα, we performed immunohistochemistry on every fifth section of the 25 consecutive sections. We measured the intensity of nuclear immunoreactivities for 8OHdG and NFκBp65 and the intensity of the cytoplasmic immunoreactivities for nitrotyrosine and pIκBα in the thoracic anterior horn of the 5 axial sections and in >500 cells in 5 randomly selected ×400 microscopic fields of the 5 sections of skeletal muscles from each group of mice ($n = 3$). We calculated the intensities by multiplying the staining concentration by cell sizes or nuclear sizes, which were quantified with WinROOF. To quantify the size of the motor neurons and the region of anti-GFAP immunoreactivity in the spinal anterior horn, we analyzed every fifth section of the 25 consecutive 6-μm-thick axial sections from the thoracic spinal cord using an image analyzer (WinROOF). To calculate the cell size of the skeletal muscles, >500 H&E stained fibers in randomly selected areas were examined using an image analyzer (WinROOF).

Cytochrome *c* oxidase staining of skeletal muscle

Cryostat sections (6 μm) were first incubated in the medium containing 0.1% manganese chloride, 0.1% hydrogen peroxide and 5.5 mM of diaminobenzidine tetrahydrochloride in 0.1 M sodium acetate pH 5.6 at 37°C for 60 min. The sections were washed in distilled water, incubated in 1% copper sulfate medium for 5 min, dehydrated in a graded ethanol series (70, 80, 90 and 100%) and cleared in xylene.

Quantitative RT-PCR

Total RNA was extracted from the cells using the RNeasy Mini Kit (Qiagen) and from mouse spinal cords and skeletal muscles using TRIzol (Invitrogen). The extracted RNA was then reverse-transcribed into first-strand cDNA using the SuperScript III First-Strand synthesis system (Invitrogen). RT-PCR was performed in a total volume of 25 μl that contained 12.5 μl of 2× QuantiTect SYBR Green PCR Master Mix and 0.3 μM of each primer (Sigma–Aldrich, MO, USA); the amplified products were detected with the iCycler system (Bio-rad Laboratories, Hercules, CA, USA). The reaction conditions were as follows: 95°C for 1 min, 40 cycles of 15 s at 94°C, 15 s at 59°C and 30 s at 72°C. The expression level of the internal control β2 microglobulin was simultaneously quantified. The following primers were used: 5′ ctgtgagaccaacagcctga 3′ and 5′ aatgcgagtggtcttccatc 3′ for the cell and mouse PPARγ, 5′ acagctccaagaccaggaaa 3′ and 5′ ctgaagtcgccatccttag 3′ for the mouse PGC1α, 5′ gtgtgagccaggatatagaaagac 3′ and 5′ aagccgaacatactgaactgc 3′ for the cell and mouse β2 microglobulin. The weight of the gene contained in each sample was equal to the log of the starting quantity, and the standardized expression level of each cell and mouse was equal to the weight ratio of each gene to that of β2 microglobulin.

Microarray analysis of the mouse spinal cord and skeletal muscle

Gene expression in the spinal cords and skeletal muscles of untreated and PG-treated AR-97Q mice was assessed using a SurePrint G3 Mouse GE 8 × 60K Microarray (Agilent Technologies, Santa Clara, CA, USA). For each group (untreated AR-97Q and PG-treated AR-97Q), we examined the male mice at 13 weeks of age. Most of the 13-week untreated AR-97Q mice were very weak and had experienced profound muscle atrophy. The RNA from the spinal cord and skeletal muscle was isolated from three mice of each group using TRIzol (Life Technologies Corporation, Carlsbad, CA, USA) according to the manufacturer's specifications. The RNA samples were purified using the PureLink™ RNA Mini Kit (Life Technologies Corporation). The cDNA

preparation, hybridization process and microarray data analysis were performed by TAKARA BIO (Otsu, Japan). The quality of total RNA was assessed with the Agilent 2100 Bioanalyzer, and the RNA integrity number values showed sufficiently high quality (ranging from 8.7 to 9.2). Agilent one-color microarray-based gene expression profiling was used to detect differential gene expression in the spinal cords and skeletal muscles of untreated and PG-treated AR-97Q mice. Array image analysis and the calculation of spot intensity measurements were performed with Agilent's Feature Extraction Software. The criteria used to detect the differences in gene expression were a 2-fold and 3-fold change in the spinal cords and muscles, respectively, of PG-treated AR-97Q mice compared with untreated AR-97Q mice. The expression profiles were analyzed using GeneSpring 12.5 software (Silicon Genetics, CA, USA). The microarray profiling data were deposited in the Gene Expression Omnibus data base with the accession number GSE51807.

Urinary analyses of the AR-97Q mice

The mice were placed in metabolic cages, and urine was collected over a 24-h period. The concentration of 8-OHdG was measured with an ELISA kit for 8-hydroxy-2′-deoxyguanosine (Japan Institute for the Control of Aging (JaICA), Shizuoka, Japan) and that of creatinine was measured with an ELISA kit for creatinine (Cayman) according to the manufacturer's instructions. The urinary levels of 8-OHdG were normalized in relation to creatinine levels to adjust for the urine volume.

Statistical analysis

We analyzed the data using the unpaired Student's *t*-test for two group comparisons and analysis of variance (ANOVA) with Dunnett's test for multiple comparisons using PASW Statistics 18 (Chicago, IL, USA). The survival rate was analyzed by Kaplan–Meier and log-rank tests using STATVIEW software version 5 (Hulinks, Tokyo, Japan). We denoted *P*-values of 0.05 or less as statistically significant.

Study approval

The collection of autopsied human tissues and their use for this study were approved by the Ethics Committee of Nagoya University Graduate School of Medicine (No. 902-3), and written informed consent was obtained from the patients' next-of-kin. Experimental procedures involving human subjects were conducted in conformance with the principles expressed in the Declaration of Helsinki. All of the animal experiments were performed in accordance with the National Institutes of Health Guide for the Care and Use of Laboratory Animals and under the approval of the Nagoya University Animal Experiment Committee (No. 25087).

SUPPLEMENTARY MATERIAL

Supplementary Material is available at *HMG* online.

ACKNOWLEDGEMENT

Pioglitazone was provided by Takeda Pharmaceutical Co., Ltd.

Conflict of Interest statement. None declared.

FUNDING

This work was supported by the Global COE Program, MEXT, Japan; MEXT/JSPS KAKENHI (grant numbers 21229011, 21689024, 22110005, 23390230, 24659428 and 26293206); Health Labor Sciences Research Grants, MHLW, Japan; CREST, JST; a grant from the Kennedy Disease Association and a grant from the Daiichi Sankyo Foundation of Life Science. The investigators had sole discretion over study design, collection, analysis, and interpretation of data, writing of the report, and decision to submit it for publication.

REFERENCES

1. La Spada, A.R. and Taylor, J.P. (2010) Repeat expansion disease: progress and puzzles in disease pathogenesis. *Nat. Rev. Genet.*, **11**, 247–258.
2. Kennedy, W.R., Alter, M. and Sung, J.H. (1968) Progressive proximal spinal and bulbar muscular atrophy of late onset. A sex-linked recessive trait. *Neurology*, **18**, 671–680.
3. Sobue, G., Hashizume, Y., Mukai, E., Hirayama, M., Mitsuma, T. and Takahashi, A. (1989) X-linked recessive bulbospinal neuronopathy. A clinicopathological study. *Brain*, **112**, 209–232.
4. Katsuno, M., Tanaka, F., Adachi, H., Banno, H., Suzuki, K., Watanabe, H. and Sobue, G. (2012) Pathogenesis and therapy of spinal and bulbar muscular atrophy (SBMA). *Prog. Neurobiol.*, **99**, 246–256.
5. Katsuno, M., Adachi, H., Kume, A., Li, M., Nakagomi, Y., Niwa, H., Sang, C., Kobayashi, Y., Doyu, M. and Sobue, G. (2002) Testosterone reduction prevents phenotypic expression in a transgenic mouse model of spinal and bulbar muscular atrophy. *Neuron*, **35**, 843–854.
6. Minamiyama, M., Katsuno, M., Adachi, H., Doi, H., Kondo, N., Iida, M., Ishigaki, S., Fujioka, Y., Matsumoto, S., Miyazaki, Y. *et al.* (2012) Naratriptan mitigates CGRP1-associated motor neuron degeneration caused by an expanded polyglutamine repeat tract. *Nat. Med.*, **18**, 1531–1538.
7. Nedelsky, N.B., Pennuto, M., Smith, R.B., Palazzolo, I., Moore, J., Nie, Z., Neale, G. and Taylor, J.P. (2010) Native functions of the androgen receptor are essential to pathogenesis in a Drosophila model of spinobulbar muscular atrophy. *Neuron*, **67**, 936–952.
8. Katsuno, M., Adachi, H., Minamiyama, M., Waza, M., Tokui, K., Banno, H., Suzuki, K., Onoda, Y., Tanaka, F., Doyu, M. *et al.* (2006) Reversible disruption of dynactin 1-mediated retrograde axonal transport in polyglutamine-induced motor neuron degeneration. *J. Neurosci.*, **26**, 12106–12117.
9. Sorarù, G., D'Ascenzo, C., Polo, A., Palmieri, A., Baggio, L., Vergani, L., Gellera, C., Moretto, G., Pegoraro, E. and Angelini, C. (2008) Spinal and bulbar muscular atrophy: skeletal muscle pathology in male patients and heterozygous females. *J. Neurol. Sci.*, **264**, 100–105.
10. Rhodes, L.E., Freeman, B.K., Auh, S., Kokkinis, A.D., La, P.A., Chen, C., Lehky, T.J., Shrader, J.A., Levy, E.W., Harris, L.M. *et al.* (2009) Clinical features of spinal and bulbar muscular atrophy. *Brain*, **132**, 3242–3251.
11. Hashizume, A., Katsuno, M., Banno, H., Suzuki, K., Suga, N., Mano, T., Atsuta, N., Oe, H., Watanabe, H., Tanaka, F. *et al.* (2012) Longitudinal changes of outcome measures in spinal and bulbar muscular atrophy. *Brain*, **135**, 2838–2848.
12. Chevalier-Larsen, E.S., O'Brien, C.J., Wang, H., Jenkins, S.C., Holder, L., Lieberman, A.P. and Merry, D.E. (2004) Castration restores function and neurofilament alterations of aged symptomatic males in a transgenic mouse model of spinal and bulbar muscular atrophy. *J. Neurosci.*, **24**, 4778–4786.
13. Palazzolo, I., Stack, C., Kong, L., Musaro, A., Adachi, H., Katsuno, M., Sobue, G., Taylor, J.P., Sumner, C.J., Fischbeck, K.H. *et al.* (2009) Overexpression of IGF-1 in muscle attenuates disease in a mouse model of spinal and bulbar muscular atrophy. *Neuron*, **63**, 316–328.
14. Yu, Z., Dadgar, N., Albertelli, M., Gruis, K., Jordan, C., Robins, D.M. and Lieberman, A.P. (2006) Androgen-dependent pathology demonstrates

myopathic contribution to the Kennedy disease phenotype in a mouse knock-in model. *J. Clin. Invest.*, **116**, 2663–2672.
15. Lieberman, A.P., Zhang, Z., Wang, J., Zhang, C., Li, H. and Xu, Y. (2014) Peripheral androgen receptor gene suppression rescues disease in mouse models of spinal and bulbar muscular atrophy. *Cell Rep.*, **7**, 774–784.
16. Cortes, C.J., Ling, S.C., Guo, L.T., Hung, G., Tsunemi, T., Ly, L., Tokunaga, S., Lopez, E., Sopher, B.L., Bennett, C.F. *et al.* (2014) Muscle expression of mutant androgen receptor accounts for systemic and motor neuron disease phenotypes in spinal and bulbar muscular atrophy. *Neuron*, **82**, 295–307.
17. Ranganathan, S., Harmison, G.G., Meyertholen, K., Pennuto, M., Burnett, B.G. and Fischbeck, K.H. (2009) Mitochondrial abnormalities in spinal and bulbar muscular atrophy. *Hum. Mol. Genet.*, **18**, 27–42.
18. Beauchemin, A.M., Gottlieb, B., Beitel, L.K., Elhaji, Y.A., Pinsky, L. and Trifiro, M.A. (2001) Cytochrome c oxidase subunit Vb interacts with human androgen receptor: a potential mechanism for neurotoxicity in spinobulbar muscular atrophy. *Brain Res. Bull.*, **56**, 285–297.
19. Cui, L., Jeong, H., Borovecki, F., Parkhurst, C.N., Tanese, N. and Krainc, D. (2006) Transcriptional repression of PGC-1 alpha by mutant huntingtin leads to mitochondrial dysfunction and neurodegeneration. *Cell*, **127**, 59–69.
20. Tontonoz, P. and Spiegelman, B.M. (2008) Fat and beyond: the diverse biology of PPARγ. *Annu. Rev. Biochem.*, **77**, 289–312.
21. Storer, P.D., Xu, J., Chavis, J. and Drew, P.D. (2005) Peroxisome proliferator-activated receptor-gamma agonists inhibit the activation of microglia and astrocytes: implications for multiple sclerosis. *J. Neuroimmunol.*, **161**, 113–122.
22. Gray, E., Ginty, M., Kemp, K., Scolding, N. and Wilkins, A. (2012) The PPAR-γ agonist pioglitazone protects cortical neurons from inflammatory mediators via improvement in peroxisomal function. *J. Neuroinflammation*, **9**, 63.
23. Xu, F., Li, J., Ni, W., Shen, Y.W. and Zhang, X.P. (2013) Peroxisome proliferator-activated receptor-γ agonist 15d-prostaglandin J2 mediates neuronal autophagy after cerebral ischemia-reperfusion injury. *PLoS One*, **8**, e55080.
24. Quintanilla, R.A., Jin, Y.N., Fuenzalida, K., Bronfman, M. and Johnson, G.V. (2008) Rosiglitazone treatment prevents mitochondrial dysfunction in mutant huntingtin-expressing cells: possible role of peroxisome proliferator-activated receptor-gamma (PPARgamma) in the pathogenesis of Huntington disease. *J. Biol. Chem.*, **283**, 25628–25637.
25. Mano, T., Katsuno, M., Banno, H., Suzuki, K., Suga, N., Hashizume, A., Tanaka, F. and Sobue, G. (2012) Cross-sectional and longitudinal analysis of an oxidative stress biomarker for spinal and bulbar muscular atrophy. *Muscle Nerve*, **46**, 692–697.
26. Zhang, H.L., Xu, M., Wei, C., Qin, A.P., Liu, C.F., Hong, L.Z., Zhao, X.Y., Liu, J. and Qin, Z.H. (2011) Neuroprotective effects of pioglitazone in a rat model of permanent focal cerebral ischemia are associated with peroxisome proliferator-activated receptor gamma-mediated suppression of nuclear factor-κB signaling pathway. *Neuroscience*, **176**, 381–395.
27. Dehmer, T., Heneka, M.T., Sastre, M., Dichgans, J. and Schulz, J.B. (2004) Protection by pioglitazone in the MPTP model of Parkinson's disease correlates with I kappa B alpha induction and block of NF kappa B and iNOS activation. *J. Neurochem.*, **88**, 494–501.
28. Mandrekar-Colucci, S., Karlo, J.C. and Landreth, G.E. (2012) Mechanisms underlying the rapid peroxisome proliferator-activated receptor-γ-mediated amyloid clearance and reversal of cognitive deficits in a murine model of Alzheimer's disease. *J. Neurosci.*, **32**, 10117–10128.
29. Chawla, A. (2010) Control of macrophage activation and function by PPARs. *Circ. Res.*, **106**, 1559–1569.
30. Trushina, E. and McMurray, C.T. (2007) Oxidative stress and mitochondrial dysfunction in neurodegenerative diseases. *Neuroscience*, **145**, 1233–1248.
31. Seong, I.S., Ivanova, E., Lee, J.M., Choo, Y.S., Fossale, E., Anderson, M., Gusella, J.F., Laramie, J.M., Myers, R.H., Lesort, M. *et al.* (2005) HD CAG repeat implicates a dominant property of huntingtin in mitochondrial energy metabolism. *Hum. Mol. Genet.*, **14**, 2871–2880.
32. Hervias, I., Beal, M.F. and Manfredi, G. (2006) Mitochondrial dysfunction and amyotrophic lateral sclerosis. *Muscle Nerve*, **33**, 598–608.
33. Browne, S.E. and Beal, M.F. (2006) Oxidative damage in Huntington's disease pathogenesis. *Antioxid. Redox Signal.*, **8**, 2061–2073.
34. Panov, A.V., Gutekunst, C.A., Leavitt, B.R., Hayden, M.R., Burke, J.R., Strittmatter, W.J. and Greenamyre, J.T. (2002) Early mitochondrial calcium defects in Huntington's disease are a direct effect of polyglutamines. *Nat. Neurosci.*, **5**, 731–736.
35. Di Prospero, N.A. and Fischbeck, K.H. (2005) Therapeutics development for triplet repeat expansion diseases. *Nat. Rev. Genet.*, **6**, 756–765.
36. Thau, N., Knippenberg, S., Körner, S., Rath, K.J., Dengler, R. and Petri, S. (2012) Decreased mRNA expression of PGC-1α and PGC-1α-regulated factors in the SOD1G93A ALS mouse model and in human sporadic ALS. *J. Neuropathol. Exp. Neurol.*, **71**, 1064–1074.
37. Eschbach, J., Schwalenstöcker, B., Soyal, S.M., Bayer, H., Wiesner, D., Akimoto, C., Nilsson, A.C., Birve, A., Meyer, T., Dupuis, L. *et al.* (2013) PGC-1α is a male-specific disease modifier of human and experimental amyotrophic lateral sclerosis. *Hum. Mol. Genet.*, **22**, 3477–3484.
38. Kiaei, M., Kipiani, K., Chen, J., Calingasan, N.Y. and Beal, M.F. (2005) Peroxisome proliferator-activated receptor-gamma agonist extends survival in transgenic mouse model of amyotrophic lateral sclerosis. *Exp. Neurol.*, **191**, 331–336.
39. Kiaei, M. (2008) Peroxisome proliferator-activated receptor-gamma in amyotrophic lateral sclerosis and huntington's disease. *PPAR Res.*, **2008**, 418765.
40. Kalonia, H., Kumar, P. and Kumar, A. (2010) Pioglitazone ameliorates behavioral, biochemical and cellular alterations in quinolinic acid induced neurotoxicity: possible role of peroxisome proliferator activated receptor-upsilon (PPARUpsilon) in Huntington's disease. *Pharmacol. Biochem. Behav.*, **96**, 115–124.
41. Park, S.W., Yi, J.H., Miranpuri, G., Satriotomo, I., Bowen, K., Resnick, D.K. and Vemuganti, R. (2007) Thiazolidinedione class of peroxisome proliferator-activated receptor gamma agonists prevents neuronal damage, motor dysfunction, myelin loss, neuropathic pain, and inflammation after spinal cord injury in adult rats. *J. Pharmacol. Exp. Ther.*, **320**, 1002–1012.
42. Landreth, G.E. and Heneka, M.T. (2001) Anti-inflammatory actions of peroxisome proliferator-activated receptor gamma agonists in Alzheimer's disease. *Neurobiol. Aging*, **22**, 937–944.
43. Wayman, N.S., Hattori, Y., McDonald, M.C., Mota-Filipe, H., Cuzzocrea, S., Pisano, B., Chatterjee, P.K. and Thiemermann, C. (2002) Ligands of the peroxisome proliferator-activated receptors (PPAR-gamma and PPAR-alpha) reduce myocardial infarct size. *FASEB J.*, **16**, 1027–1040.
44. Liu, H.R., Tao, L., Gao, E., Lopez, B.L., Christopher, T.A., Willette, R.N., Ohlstein, E.H., Yue, T.L. and Ma, X.L. (2004) Anti-apoptotic effects of rosiglitazone in hypercholesterolemic rabbits subjected to myocardial ischemia and reperfusion. *Cardiovasc. Res.*, **62**, 135–144.
45. Bright, J.J., Kanakasabai, S., Chearwae, W. and Chakraborty, S. (2008) PPAR regulation of inflammatory signaling in CNS diseases. *PPAR Res.*, **2008**, 658520.
46. Dupuis, L., Dengler, R., Heneka, M.T., Meyer, T., Zierz, S., Kassubek, J., Fischer, W., Steiner, F., Lindauer, E., Otto, M. *et al.* (2012) A randomized, double blind, placebo-controlled trial of pioglitazone in combination with riluzole in amyotrophic lateral sclerosis. *PLoS One*, **7**, e37885.
47. Hunt, M.J. and Morton, A.J. (2005) Atypical diabetes associated with inclusion formation in the R6/2 mouse model of Huntington's disease is not improved by treatment with hypoglycaemic agents. *Exp. Brain Res.*, **166**, 220–229.
48. Di Filippo, M., Chiasserini, D., Tozzi, A., Picconi, B. and Calabresi, P. (2010) Mitochondria and the link between neuroinflammation and neurodegeneration. *J. Alzheimers Dis.*, **20**, S369–S379.
49. Stommel, E.W., Van Hoff, R.M., Graber, D.J., Bercury, K.K., Langford, G.M. and Harris, B.T. (2007) Tumor necrosis factor-alpha induces changes in mitochondrial cellular distribution in motor neurons. *Neuroscience*, **146**, 1013–1019.
50. Mauro, C., Leow, S.C., Anso, E., Rocha, S., Thotakura, A.K., Tornatore, L., Moretti, M., De Smaele, E., Beg, A.A., Tergaonkar, V. *et al.* (2011) NF-κB controls energy homeostasis and metabolic adaptation by upregulating mitochondrial respiration. *Nat. Cell. Biol.*, **13**, 1272–1279.
51. Mariappan, N., Elks, C.M., Sriramula, S., Guggilam, A., Liu, Z., Borkhsenious, O. and Francis, J. (2010) NF-kappaB-induced oxidative stress contributes to mitochondrial and cardiac dysfunction in type II diabetes. *Cardiovasc. Res.*, **85**, 473–483.
52. Kaltschmidt, B. and Kaltschmidt, C. (2009) NF-kappaB in the nervous system. *Cold Spring Harb. Perspect. Biol.*, **1**, a001271.
53. Swarup, V., Phaneuf, D., Dupré, N., Petri, S., Strong, M., Kriz, J. and Julien, J.P. (2011) Deregulation of TDP-43 in amyotrophic lateral sclerosis triggers nuclear factor κB-mediated pathogenic pathways. *J. Exp. Med.*, **208**, 2429–2447.
54. Yates, L.L. and Górecki, D.C. (2006) The nuclear factor-kappaB (NF-kappaB): from a versatile transcription factor to a ubiquitous therapeutic target. *Acta Biochim. Pol.*, **53**, 651–662.

55. Sambataro, F. and Pennuto, M. (2012) Cell-autonomous and non-cell-autonomous toxicity in polyglutamine diseases. *Prog. Neurobiol.*, **97**, 152–172.
56. Ilieva, H., Polymenidou, M. and Cleveland, D.W. (2009) Non-cell autonomous toxicity in neurodegenerative disorders: ALS and beyond. *Cell Biol.*, **187**, 761–772.
57. Boillée, S., Yamanaka, K., Lobsiger, C.S., Copeland, N.G., Jenkins, N.A., Kassiotis, G., Kollias, G. and Cleveland, D.W. (2006) Onset and progression in inherited ALS determined by motor neurons and microglia. *Science*, **312**, 1389–1392.
58. Beers, D.R., Henkel, J.S., Zhao, W., Wang, J. and Appel, S.H. (2008) CD4+ T cells support glial neuroprotection, slow disease progression, and modify glial morphology in an animal model of inherited ALS. *Proc. Natl. Acad. Sci. USA*, **105**, 15558–15563.
59. Henkel, J.S., Beers, D.R., Siklós, L. and Appel, S.H. (2006) The chemokine MCP-1 and the dendritic and myeloid cells it attracts are increased in the mSOD1 mouse model of ALS. *Mol. Cell. Neurosci.*, **31**, 427–437.
60. Kishida, K., Shimomura, I., Nishizawa, H., Maeda, N., Kuriyama, H., Kondo, H., Matsuda, M., Nagaretani, H., Ouchi, N., Hotta, K. *et al.* (2001) Enhancement of the aquaporin adipose gene expression by a peroxisome proliferator-activated receptor gamma. *J. Biol. Chem.*, **276**, 48572–48579.
61. Waza, M., Adachi, H., Katsuno, M., Minamiyama, M., Sang, C., Tanaka, F., Inukai, A., Doyu, M. and Sobue, G. (2005) 17-AAG, an Hsp90 inhibitor, ameliorates polyglutamine-mediated motor neuron degeneration. *Nat. Med.*, **11**, 1088–1095.
62. Katsuno, M., Adachi, H., Minamiyama, M., Waza, M., Doi, H., Kondo, N., Mizoguchi, H., Nitta, A., Yamada, K., Banno, H. *et al.* (2010) Disrupted transforming growth factor-beta signaling in spinal and bulbar muscular atrophy. *J. Neurosci.*, **30**, 5702–5712.
63. Kobayashi, Y., Kume, A., Li, M., Doyu, M., Hata, M., Ohtsuka, K. and Sobue, G. (2000) Chaperones Hsp70 and Hsp40 suppress aggregate formation and apoptosis in cultured neuronal cells expressing truncated androgen receptor protein with expanded polyglutamine tract. *J. Biol. Chem.*, **275**, 8772–8778.
64. Adachi, H., Waza, M., Tokui, K., Katsuno, M., Minamiyama, M., Tanaka, F., Doyu, M. and Sobue, G. (2007) CHIP overexpression reduces mutant androgen receptor protein and ameliorates phenotypes of the spinal and bulbar muscular atrophy transgenic mouse model. *J. Neurosci.*, **27**, 5115–5126.
65. Kondo, N., Katsuno, M., Adachi, H., Minamiyama, M., Doi, H., Matsumoto, S., Miyazaki, Y., Iida, M., Tohnai, G., Nakatsuji, H. *et al.* (2013) Heat shock factor-1 influences pathological lesion distribution of polyglutamine-induced neurodegeneration. *Nat. Commun.*, **4**, 1405.
66. Toyokuni, S., Tanaka, T., Hattori, Y., Nishiyama, Y., Yoshida, A., Uchida, K., Hiai, H., Ochi, H. and Osawa, T. (1997) Quantitative immunohistochemical determination of 8-hydroxy-2′-deoxyguanosine by a monoclonal antibody N45.1: its application to ferric nitrilotriacetate-induced renal carcinogenesis model. *Lab. Invest.*, **76**, 365–374.

Evaluation of *SLC20A2* mutations that cause idiopathic basal ganglia calcification in Japan

Megumi Yamada, MD*
Masaki Tanaka, MD*
Mari Takagi, BA
Seiju Kobayashi, MD, PhD
Yoshiharu Taguchi, MD, PhD
Shutaro Takashima, MD, PhD
Kortaro Tanaka, MD, PhD
Tetsuo Touge, MD, PhD
Hiroyuki Hatsuta, MD
Shigeo Murayama, MD, PhD
Yuichi Hayashi, MD, PhD
Masayuki Kaneko, PhD
Hiroyuki Ishiura, MD, PhD
Jun Mitsui, MD, PhD
Naoki Atsuta, MD, PhD
Gen Sobue, MD, PhD
Nobuyuki Shimozawa, MD, PhD
Takashi Inuzuka, MD, PhD
Shoji Tsuji, MD, PhD
Isao Hozumi, MD, PhD

Correspondence to Dr. Hozumi: hozumi@gifu-pu.ac.jp

Supplemental data at www.neurology.org

ABSTRACT

Objective: To investigate the clinical, genetic, and neuroradiologic presentations of idiopathic basal ganglia calcification (IBGC) in a nationwide study in Japan.

Methods: We documented clinical and neuroimaging data of a total of 69 subjects including 23 subjects from 10 families and 46 subjects in sporadic cases of IBGC in Japan. Mutational analysis of *SLC20A2* was performed.

Results: Six new mutations in *SLC20A2* were found in patients with IBGC: 4 missense mutations, 1 nonsense mutation, and 1 frameshift mutation. Four of them were familial cases and 2 were sporadic cases in our survey. The frequency of families with mutations in *SLC20A2* in Japan was 50%, which was as high as in a previous report on other regions. The clinical features varied widely among the patients with *SLC20A2* mutations. However, 2 distinct families have the same mutation of S637R in *SLC20A2* and they have similar characteristics in the clinical course, symptoms, neurologic findings, and neuroimaging. In our study, all the patients with *SLC20A2* mutations showed calcification. In familial cases, there were symptomatic and asymptomatic patients in the same family.

Conclusion: *SLC20A2* mutations are a major cause of familial IBGC in Japan. The members in the families with the same mutation had similar patterns of calcification in the brain and the affected members showed similar clinical manifestations. ***Neurology*® 2014;82:1–8**

GLOSSARY

DNTC = diffuse neurofibrillary tangles with calcification; **FIBGC** = familial idiopathic basal ganglia calcification; **IBGC** = idiopathic basal ganglia calcification; **MMSE** = Mini-Mental State Examination; **PDGF** = platelet-derived growth factor; **PDGFRB** = platelet-derived growth factor receptor-β; **Pi** = inorganic phosphate; **PiB** = Pittsburgh compound B; **PiT** = type III sodium-dependent phosphate transporter; **PKC** = paroxysmal kinesigenic choreoathetosis.

Idiopathic basal ganglia calcification (IBGC), also known as Fahr disease, is thought to be a rare neuropsychiatric disorder characterized by symmetrical calcification in the basal ganglia and other brain regions. Clinical manifestations range widely from asymptomatic to variable symptoms including headaches, psychosis, and dementia.[1] The diagnosis of IBGC generally relies on the visualization of bilateral calcification mainly in the basal ganglia by neuroimaging and the absence of metabolic, infectious, toxic, or traumatic causes.[2,3]

The mode of inheritance of familial IBGC (FIBGC) has been thought to be autosomal dominant and, to date, 4 responsible chromosomal regions have been identified, namely 14q (IBGC1), 2q37 (IBGC2), 8p11.21 (IBGC3), and 5q32 (IBGC4).[3–14] The causative gene at the IBGC3 locus was identified as *SLC20A2* encoding type III sodium-dependent phosphate transporter 2 (PiT-2). Screening of a large series of patients with IBGC revealed that mutations in *SLC20A2* are a major cause of FIBGC[10]; moreover, other mutations in *SLC20A2* have recently been reported in China and Brazil.[11–13] The mutations of *PDGFRB* encoding platelet-derived growth factor

*These authors contributed equally to this work.

From the Laboratory of Medical Therapeutics and Molecular Therapeutics (Y.M., M. Takagi, Y.H., M.K., I.H.), Gifu Pharmaceutical University, Gifu; Department of Neurology (M. Tanaka, H. I., J.M., S. Tsuji), The University of Tokyo; Department of Neurology (N.A., G.S.), Nagoya University; Department of Neuropsychiatry (S.K.), Sapporo Medical University, Sapporo; Department of Neurology (Y.Y., S. Takashima, K.T.), Toyama University Hospital, Toyama; Department of Neurology (T.T.), Kagawa University Hospital, Kagawa; Department of Neurology (H.H, S.M.), Tokyo Metropolitan Institute of Gerontology, Tokyo; Department of Neurology and Geriatrics (M.Y., Y.H., T.I.), and Division of Genomic Research, Life Science Research Center (N.S.), Gifu University, Gifu, Japan.

Go to Neurology.org for full disclosures. Funding information and disclosures deemed relevant by the authors, if any, are provided at the end of the article.